BeBeC-2018-D07

IMPROVING SOURCE DISCRIMINATION PERFORMANCE BY USING AN OPTIMIZED ACOUSTIC ARRAY AND ADAPTIVE HIGH-RESOLUTION CLEAN-SC BEAMFORMING

Salil Luesutthiviboon[1], Anwar Malgoezar[1], Mirjam Snellen[1],
Pieter Sijtsma[1,2], and Dick Simons[1]
[1]Section Aircraft Noise & Climate Effects (ANCE)
Faculty of Aerospace Engineering, Delft University of Technology
Kluyverweg 1, 2629 HS, Delft, the Netherlands
[2]Pieter Sijtsma Advanced AeroAcoustics (PSA3)
Princes Margrietlaan 13, 8091 AV, Wezep, the Netherlands

Abstract

Beamforming performance can be improved in two ways: optimizing the location of microphones on the acoustic array and applying advanced beamforming algorithms. In this study, the effects of the two approaches are studied. An optimization method is developed to optimize the location of microphones for an acoustic array used in an open-jet anechoic wind tunnel. Then the benefits of using the optimized array with the recently-developed advanced beamforming algorithm, the High-Resolution (HR) CLEAN-SC algorithm are investigated. The microphone locations were optimized to obtain both good resolution and low side lobe levels. By using the optimized array and applying the HR CLEAN-SC algorithm, it was found that two closely-spaced sound sources can be resolved in a broad frequency range below the Rayleigh limit. The findings have also been confirmed through experimental validation.

1 INTRODUCTION

Acoustic arrays and beamforming algorithms have been employed in many acoustic studies. After applying beamforming, *source maps* which visualize, quantify, and localize sources of sound in a region of interest, are obtained. In aerospace and aeroacoustic studies, this has been used in various aspects, ranging from outdoor beamforming of fly-over aircraft [1], to beamforming for aeroacoustic studies in wind tunnels [2]. Further investigations of the source maps help researchers to understand characteristics of contributing noise sources. The insights

obtained can be used to achieve improved designs with lower noise emission, such as airfoils with reduced noise [3].

Ideal source maps should visualize the sound sources at their correct locations. When there are multiple sources, the sources should be separable. Moreover, false source idendifications due to side lobes should be minimized. These qualities in the source maps indicate the *beamforming performance*, and can be improved by two ways. First, the location of the microphones on the acoustic array can be strategically synthesized [4] or optimized [5–7]. Second, advanced beamforming algorithms can be applied when post-processing the acquired signals. So far, these two aspects have been done separately. The interplay between optimized array designs and advanced beamforming algorithms has not yet been investigated.

An advanced beamforming algorithm, the High-Resolution (HR) CLEAN-SC, has recently been introduced [8]. This method is an extension of the CLEAN-SC algorithm [9] and is able to resolve closely spaced sound sources. However, the performance of it depends on the quality of the array design. Therefore, this study aims to improve the beamforming performance of an acoustic array with the focus on optimizing the design of the microphone configuration. Once the beamforming performance of the optimized array configuration is proven to be inherently good through the application of the conventional beamforming algorithm, the effects of using the optimized array design on the beamforming performance of the HR CLEAN-SC algorithm are studied.

The acoustic array used in this study is a planar 2×2 m acoustic array holding 64 microphones. The array is installed in the 'V-tunnel' facility at Delft University of Technology, which is an open-jet anechoic wind tunnel for aeroacoustic studies. Moreover, experimental validation has also been done in this facility.

This paper is structured as follows: In Section 2, the parameters for quantifying the source map quality are introduced. The state-of-the-art acoustic array microphone placement optimization methods and beamforming methods are summarized. Section 3 discusses the optimization method proposed for this work. Next, the optimization results are presented in Section 4. The results of applying the HR CLEAN-SC algorithm using an optimized array are investigated through beamforming simulations. Section 5 provides the results from the experimental validation. Finally, conclusions and recommendations are given in Section 6.

2 IMPROVING BEAMFORMING PERFORMANCE

2.1 Quantifying beamforming performance

The parameters used to describe the beamforming performance of an array can be derived from the source map it produces. To generalize this explanation, an analytical source map produced by a finite-aperture circular array with the diameter D having an infinite number of microphones is used. Supposing that the array is centered at the coordinate $(x,y,z) = (0,0,0)$ and there is a point source placed on a plane at the coordinate $(x,y,z) = (0,0,h)$ as shown in Fig. 1, the array will resolve this point source in an analogous way as in optics, where light is focused by a circular lens to a spot and a pattern of low-intensity light around it due to diffraction [5]. This pattern is called the *Point Spread Function* (PSF) or the *Airy Pattern*. For a beamforming frequency f and a plane wave assumption, the PSF can be written as

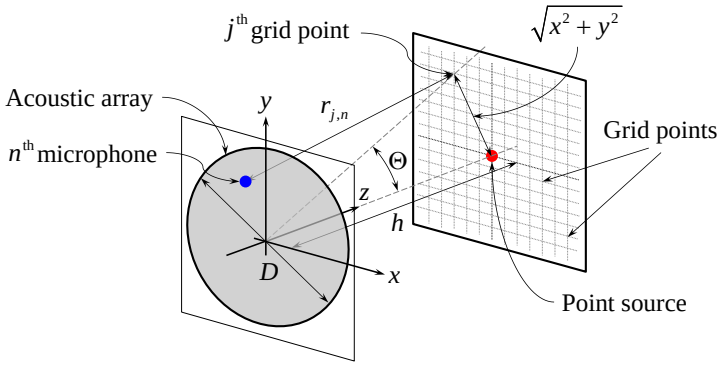

Figure 1: Notations used in analytical PSF calculation and beamforming

$$A(\Theta) = \left[\frac{2J_1(\frac{\pi f D}{c}\sin(\Theta))}{\frac{\pi f D}{c}\sin(\Theta)}\right]^2, \tag{1}$$

where J_1 is the Bessel function of the first kind, c is the speed of sound, and Θ is the angle measured from the array's center to the point of interest, $\Theta = \tan^{-1}(\frac{\sqrt{x^2+y^2}}{h})$.

In beamforming, the plane where the source lies on is discretized into grid points. For any grid points, (x,y,z), the source autopower (A) can be determined. For this exemplary case, the Sound Pressure Level (SPL) at the j^{th} grid point in decibels (dB) is

$$SPL_j = 10\log_{10}[A(\Theta)/p_{\text{ref}}^2], \tag{2}$$

where p_{ref} is the reference pressure of 2×10^{-5} Pa. Assuming a source of 2×10^{-5} Pa, this is visualized in Fig. 2. The resulting SPL in plane $X-Z$ is also shown. It can be seen that the source map consists of a series of lobes. The lobe with the highest peak represents the sound source. This lobe is called the *main lobe*. Since the source is actually a point source, it is desirable to have as narrow as possible main lobe in order to better localize the source and distinguish this source from another source when they are placed closely together, i.e. having a high resolution. The parameter *Main Lobe Width* (MLW) is defined to measure this quality of the array. The MLW is usually defined as the width of the main lobe at SPL = -3 dB relative to the main lobe's peak [4, 6]. In a three-dimensional plot, the MLW is the maximum distance between a pair of points representing the main lobe's -3 dB contour.

Apart from the main lobe, there is a series of lobes around it which do not represent any sound sources. These are the so-called *side lobes*. When the level of the side lobes is high, they are more likely to be misinterpreted as true sound sources. Therefore, it is ideal that their levels are as low as possible. To measure this quality, the *Maximum Side lobe Level* (MSL) is defined as the relative SPL of the main lobe's peak and the highest side lobe's peak [6]. This analytical case, where the number of microphones is infinite, also shows that the minimum attainable MSL is approximately -17.6 dB.

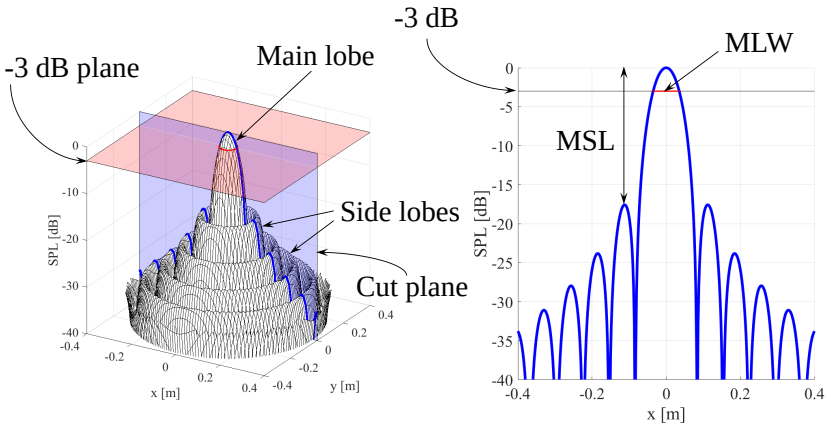

Figure 2: Source map resolved by a finite-aperture array with infinite number of microphones and definitions of MSL and MLW

2.2 Improving beamforming performance by acoustic array optimization

In reality, the number of microphones on the acoustic array is finite. Because of that, the beamforming performance will deviate from the ideal-case shown in Fig. 2, i.e. having higher MLW and MSL. Microphone placement optimization is usually done to obtain low MLW and MSL.

Many studies have shown that lower MSL can be obtained by having the microphones densely distributed close to the array's center. In contrast, when the microphones are more densely placed close to the array's edge, the MLW decreases at the cost of increasing MSL [6, 10]. Therefore, the aim is to search for an array design which gives the best trade-off between these two qualities [4, 7, 11].

It has been found that acoustic arrays with microphones arranged in a multi-arm spiral manner can potentially give the best trade-off between MSL and MLW [10]. More specifically, for an array with 64 microphones, multi-arm spiral arrays with nine arms and seven microphones per arm (plus one microphone in the center) are likely to give the lowest MSL and MLW [7]. Apart from that, it is also known that the distance from each particular microphone to its nearest-neighbor microphone can be linked to the side lobe suppression ability when beamforming is performed at a specific frequency [5].

When an array is designed to be used in particular applications, design optimization is usually performed. For this, random search evolutionary algorithms such as Genetic Algorithm (GA) [6, 12], Differential Evolution (DE) [5], and Particle Swarm Optimization (PSO) [11] can be used. One common feature among these algorithms are that they evaluate a set of multiple designs in each iteration. This process can be time-consuming and sometimes does not lead to satisfactory results. One way to facilitate the optimization process is to utilize the known relationship between the array's geometric features and the beamforming performance. For example, instead of parametrizing the location of every single microphone in the optimization, the microphone locations can be collectively defined by some parameters which correlates to MLW and MSL [4, 13]. With a reduced number of acoustic array design variables, the optimiza-

tion process can provide acoustic array designs with satisfactory performance with a reduced computational effort.

2.3 Improving beamforming performance by advanced beamforming algorithms

The beamforming performance can also be improved in the post-processing steps by applying advanced beamforming algorithms. This paper focuses on the newly-introduced HR CLEAN-SC algorithm [8] which is an extension of the CLEAN algorithms [9].

Conventional beamforming works by assuming that there is a potential sound source at each scan point. Then the sound propagation from that scan point is modelled. The estimated source power at the j^{th} grid point ($\tilde{A}_j$) is obtained by minimizing the errors between the acquired signal and the modelled signal. The final expression for the estimated source power in conventional beamforming is

$$\tilde{A}_j = \mathbf{w}_j^* \mathbf{C} \mathbf{w}_j, \tag{3}$$

where $*$ represents the complex conjugate transpose. The matrix $\mathbf{C}$ is the *Cross Spectral Matrix* (CSM) which is expressed as

$$\mathbf{C} = \mathbf{p}\mathbf{p}^*. \tag{4}$$

The vector $\mathbf{p}$ contains the Fourier transform of the received signal at each microphone. The symbol $\mathbf{w}_j$ in Eq. (3) is the *weight vector* which reads

$$\mathbf{w}_j = \frac{\mathbf{g}_j}{\|\mathbf{g}_j\|^2}, \tag{5}$$

where $\mathbf{g}_j$ is the *steering vector*, which contains expressions for modelling the signal travelling from the j^{th} grid point to each microphone. There exist different ways of modelling the signal [14]. One frequently-used expression is [8]

$$g_{j,n} = \frac{-1}{4\pi r_{j,n}} \exp\left(\frac{-2\pi i f r_{j,n}}{c}\right), \tag{6}$$

where n is the index of microphone and $r_{j,n}$ is the distance from the j^{th} grid point to the n^{th} microphone, cf. Fig. 1.

The side lobe pattern in the source map produced by conventional beamforming is dependent on the microphone arrangement and the location of the main lobe [9, 15]. In other words, the side lobe pattern in the source map is spatially *coherent* with the sound source's location. The CLEAN-SC beamforming method, where SC stands for (spatial) *Source Coherence*, makes use of this fact by identifying the sound source (the peak) in the source map, substracting the influence of that source from the CSM, and replacing the source's contribution in the source map with a *clean* beam [9].

Let the subscript '1' denote the grid point where the estimated source power from conventional beamforming is the highest ($\tilde{A}_1$), $\mathbf{w}_1$ is the weight vector associated with this grid point. The *source component* ($\mathbf{h}_1$) is calculated from

$$\mathbf{h}_1 = \frac{\mathbf{C}\mathbf{w}_1}{\mathbf{w}_1^* \mathbf{C}\mathbf{w}_1}. \tag{7}$$

From this point, the measured CSM in Eq. (4) is assumed to be the result of contributions from K incoherent sources. The following model is introduced:

$$\mathbf{C} = \sum_{k=1}^{K} \mathbf{p}_k \mathbf{p}_k^*. \tag{8}$$

This then results in

$$\mathbf{h}_1 = \frac{\mathbf{p}_1^* \mathbf{w}_1}{\tilde{A}_1} \Big[\mathbf{p}_1 + \frac{1}{\mathbf{p}_1^* \mathbf{w}_1} \sum_{k=2}^{K} (\mathbf{p}_k^* \mathbf{w}_1) \mathbf{p}_k \Big]. \tag{9}$$

The source component represents the contribution of the identified source in the CSM. The *degraded* CSM ($\mathbf{C}_{\text{degraded}}$) which excludes the influence of this source is

$$\mathbf{C}_{\text{degraded}} = \mathbf{C} - \phi \tilde{A}_1 \mathbf{h}_1^* \mathbf{h}_1, \tag{10}$$

where ϕ is the *loop gain* or the *damping factor*, $0 < \phi \leq 1$. With this new CSM, the new source map is obtained by summing the clean beams from all identified sources with the source map produced by the remaining degraded CSM:

$$\tilde{A}_j = \sum_{k=1}^{K} \phi \tilde{A}_k 10^{-\lambda d_{j,k}^2} + \mathbf{w}_j^* \mathbf{C}_{\text{degraded}} \mathbf{w}_j. \tag{11}$$

The first term on the RHS of Eq. (11) represents the clean beams from K identified sound sources, where λ is a clean beam shape parameter and $d_{j,k}$ is the distance from the j^{th} grid point to the identified k^{th} source location. The process presented from Eq. (7) to (11) is repeated, and stopped when $\|\mathbf{C}_{\text{degraded}}\| \ll \|\mathbf{C}\|$.

The CLEAN-SC method improves the source map's quality both in terms of MLW and MSL. The MLW can freely be defined by selecting the clean beam shape parameter (λ) while the MSL is lowered by eliminating the side lobes which are spatially coherent to the main lobe.

The difference between HR CLEAN-SC and CLEAN-SC is that the HR CLEAN-SC method allows the *marking* of the source to not exactly be at the grid point where the estimated source power is the highest, i.e. $\mathbf{w}_1$ may not be used. Alternatively, the HR CLEAN-SC attempts to put the identified source marker at the grid point where the relative contribution of the other sources' PSF(s) is the lowest [8]. The HR CLEAN-SC algorithm works with the known number of sources (K) identified by the CLEAN-SC algorithm. For each source, the weight vector ($\mathbf{w}_k$) is replaced by a new weight vector $\mathbf{u}_j$, where j is associated with a grid point which minimizes the cost function:

$$F_j(\mathbf{u}_j) = \frac{\| \sum_{k=1, k\neq j}^{K} (\mathbf{g}_k^* \mathbf{u}_j) \|^2}{|\mathbf{g}_j^* \mathbf{u}_j|^2 \|\mathbf{g}_j\|^2}. \tag{12}$$

Having found the minimizer ($\mathbf{u}_j$), the source component can be determined by

$$\mathbf{h}_j = \frac{\mathbf{C}\mathbf{u}_j}{\mathbf{u}_j^* \mathbf{C}\mathbf{u}_j}. \tag{13}$$

The contribution of the source in the source map in terms of source power is

$$\tilde{A}_j = (\mathbf{u}_j^* \mathbf{C}\mathbf{u}_j)|\mathbf{w}_j^* \mathbf{h}_j|^2. \tag{14}$$

The grid point where $\tilde{A}_j$ is maximized is the exact location of the source. The maximum value of $\tilde{A}_j$ is the source power estimate which is used to construct a clean beam (same manner as in the RHS of Eq. (11)) to represent the source at this location. The iteration process repeats Eq. (12) to (14) for all predefined number of sources until the minimizer ($\mathbf{u}_j$) for all sources no longer moves or until the maximum number of iterations is reached.

The fact that the HR CLEAN-SC algorithm allows a flexible source marker location makes it able to improve the beamforming performance in terms of resolution. In general, there exists a minimum separation limit of closely spaced sources, below which the sources cannot be resolved by a finite-aperture array using the previously-mentioned beamforming algorithms. This is the so-called *Rayleigh limit* which can be derived as follows:

Point sound sources are resolved by a finite-aperture array in form of a PSF as in Eq. (1). When the peak of the source's PSF of one source is closer than the first zero crossing of another source's PSF, these two sources are no longer resolvable. The first zero crossing occurs when the Bessel function in the numerator of Eq. (1) is zero. Let $\Theta_{\min}$ denote the minimum angle Θ where two sources are resolvable, $J_1(\frac{\pi fD}{c}\sin\Theta_{\min}) = 0$ when $\frac{\pi fD}{c}\sin\Theta_{\min} = 3.83$. Using small angle approximation, we have

$$\Theta_{\min} = 1.22\frac{c}{fD}. \tag{15}$$

Let *RL* be the Rayleigh limit, it can be written in terms of h as

$$RL = h\tan(1.22\frac{c}{fD}). \tag{16}$$

When two sources are placed closer than the Rayleigh limit, the HR CLEAN-SC algorithm shifts the source marker of each source to be at the point where the influence of the other source's PSF is the lowest. That point is therefore above the first zero crossing of the other source, which is the Rayleigh limit. With this principle, these two sources can still be resolved.

However, the selection of the new source marker is constrained by the denominator of Eq. (12). To avoid division by zero, the term $|\mathbf{g}_j^* \mathbf{u}_j|^2$ should be greater than zero. In addition, the marker should still lie on the main lobe [8]. Thus, the minimum limit of $|\mathbf{g}_j^* \mathbf{u}_j|^2$ should be set. Let μ denote this limit, a constraint can be set for the minimization problem in Eq. (12) as

$$|\mathbf{g}_j^* \mathbf{u}_j|^2 \geq \mu > 0. \tag{17}$$

The working principle of the HR CLEAN-SC algorithm can be graphically explained using Fig. 3. First, consider PSF 1 and PSF 2. The peak of PSF 1 is above the first zero-crossing of PSF 2 and vice versa. By employing conventional beamforming, this is the minimum distance where PSF 1 and PSF 2 are resolvable, i.e. the Rayleigh limit (*RL*). Next, supposing that, instead of PSF 2, there exists PSF 3 which has the peak closer to PSF 1 than *RL*, the HR CLEAN-SC

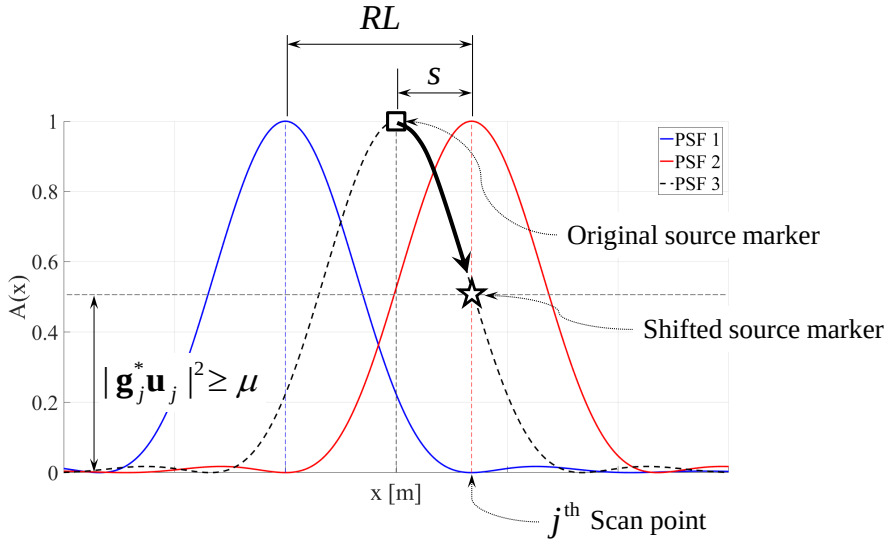

Figure 3: Rayleigh limit and the working principle of HR CLEAN-SC

algorithm shifts the marker of PSF 3 from the peak of PSF 3 to the point where the influence of PSF 1 is minimized, i.e. the first zero-crossing of PSF 1. Then PSF 1 and PSF 3 can still be resolved.

Let the source marker be shifted to the j^{th} scan point and s be the distance where the marker is shifted, the value of PSF 3 at this point is $|\mathbf{g}_j^* \mathbf{u}_j|^2 \geq \mu$. It can be seen that when μ is lower, the marker is allowed to shift further and the sources are resolvable even though they are placed closer together. However, too low a value of μ will allow the marker to stay on the side lobes, which is not desirable. Thus, an array with low side lobes will allow a lower value of μ to be selected and therefore a higher resolution improvement.

When the selected value of μ allows the source marker to shift to the maximum distance of $s_{\max}$, the *new* Rayleigh limit is potentially

$$RL_{\text{new}} = RL - s_{\max}. \tag{18}$$

Finally, the *resolution enhancement* ($\Psi \geq 1$) is defined to indicate the potential improvement in resolution due to the selected value of μ as

$$\Psi = \frac{RL}{RL_{\text{new}}} = \frac{RL}{RL - s_{\max}} \geq 1. \tag{19}$$

3 ACOUSTIC ARRAY DESIGN OPTIMIZATION METHOD

The concept of the optimization method to be described in this paper is to use a minimum number of design variables to shorten the optimization time. To achieve that, the formulated optimization problem links geometric parameters of the acoustic array directly to the beamforming performance; such as the microphone distribution density along the array's radial distance. Apart from that, weighing is applied to the side lobes, aiming to minimize the side lobe levels close to the main lobe so that the array is suitable for the HR CLEAN-SC algorithm.

A schematic diagram of the optimization routine is illustrated in Fig. 4. There are two optimization loops; the main and the nested loop. The main optimization loop has four design variables which are used to describe the microphone distribution as a function of the array's radial distance, and the distances between every pair of nearest neighboring microphones in relation to the microphone's radial distance on the array. The nested optimization loop has eleven design variables which are used to generate a set of multi-arm spiral arrays, which have the geometry as close as possible to that defined by the main loop. The beamforming performance of the generated arrays is then determined by beamforming simulation. It is hypothesized that the arrays generated by the same set of design variables from the main optimization loop will have similar performance, i.e. will cluster in the same area when plotted as shown on the right side of Fig. 4. The main optimization loop attempts to find the optimal design variables which gives as low as possible MLW and weighted MSL. The optimized array can be selected from the set of arrays generated by these optimal variables. Further details of both optimization loops are given in the following paragraphs.

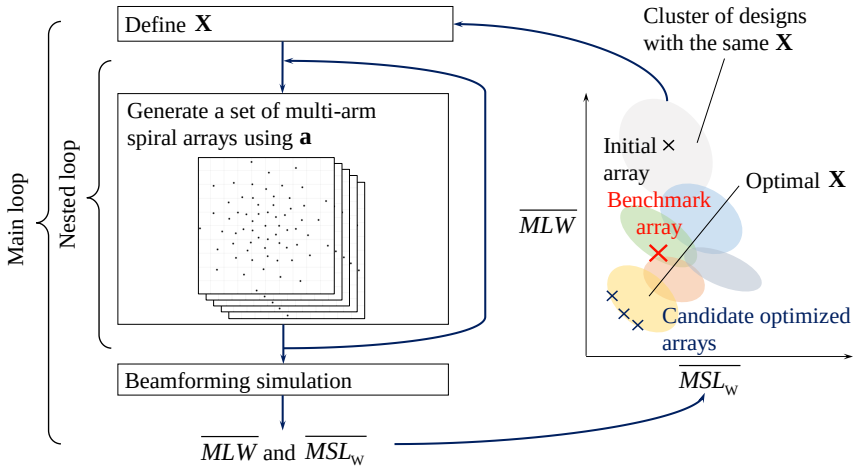

Figure 4: Schematic diagram of the optimization method used

The design vector of the main optimization loop (**X**) consists of four design variables which affect the descriptions of the array's geometry as follows:

- X_1 and X_2 describe the microphone distribution density along the array's radial distance
  - X_1 indicates the radial location of the microphone density distribution peak
  - X_2 indicates the standard deviation of the microphone density distribution
- X_3 and X_4 describe the geometry of a curve that represents the relationship between the microphone's radial distance on the array and the distance from that microphone to its nearest neighboring microphone. It is assumed that the further the microphone is from the array's center, the further it is from its nearest neighboring microphone.
  - X_3 indicates the location of the curve's inflection point
  - X_4 indicates the smoothness of the curve

This design vector is used in the optimization loop to control the generation of the arrays. Having obtained a set of arrays that satisfy these design variables, the arrays' beamforming performance is evaluated by beamforming simulation.

The beamforming simulation considers a point source emitting white noise at $h = 1.5$ m aligned with the array's center. Although the intended scan plane size in real applications is 1×1 m, the scan plane used in the optimization is a circular area with the diameter of 2 m to account for the uncertainty of the source's location. The design frequencies of the array range from 1 to 10 kHz. The MLW is evaluated only at 1 kHz. The MSL is evaluated at 4 to 10 kHz with a step of 1 kHz. The MSL is also linearly weighted according to its distance from the main lobe; the closer it is to the main lobe, the more weight it gets.

Let $\overline{MLW}$ and $\overline{MSL_{\mathrm{w}}}$ represent the averaged MLW and weighted MSL from all arrays at all relevant frequencies generated by a certain $\mathbf{X}$, the main optimization loop attempts to minimize the objective function:

$$J_{\mathrm{main}} = \frac{\overline{MLW} - MLW_{\mathrm{ref}}}{MLW_{\mathrm{ref}}} + \frac{\overline{MSL_{\mathrm{w}}} - MSL_{\mathrm{w,\,ref}}}{-MSL_{\mathrm{w,\,ref}}}, \tag{20}$$

where the subscript 'ref' represents the reference values of MLW and MSL. In each term of the objective function, the averaged value is substracted by the reference value. With this, the further it is from the reference value, the higher J_{main} becomes. The division by the reference values scales the evaluated differences of MLW and MSL, and allows the summation of these qualities, which have different units.

Although the optimization in the main loop contains only four design variables, the objective function evaluation is computationally expensive since it requires beamforming simulations. Therefore, an optimization algorithm, which has a potential to handle this requirement, should be selected. In this case, the *Generalized Pattern Search* (GPS) [16] or the *Hooke-Jeeves* (HJ) [17] algorithm was used. The detailed explanation of these algorithms can be found in [16–18].

The task of the nested optimization loop is to generate coordinates of acoustic arrays which have the geometry closest to that defined by the design vector of the main optimization loop ($\mathbf{X}$). To confine the number of the design variables used and to limit the optimization to only potential designs, the acoustic arrays are set to be multi-arm spiral arrays with nine arms and seven microphones per arm (plus one microphone in the center). For acoustic arrays with 64 microphones, this been found to achieve the best performance [7].

The design vector ($\mathbf{a}$) for the nested optimization loop has eleven design variables. They are linked to the microphone locations on one spiral arm. Once the location of all microphones on this arm is defined, the remaining microphone coordinates on this array can be obtained by equiangular rotation. The design variables in $\mathbf{a}$ specify the microphone locations on the first spiral arm as follows:

- a_1 specifies the radial distance of the innermost microphone measured from the array's center
- a_2 specifies the angular distance of the outermost microphone measured from the array's center (The radial distance of this microphone is fixed at 0.95 m, corresponding to the array's size.)
- a_3 and a_5 specify the radial distances of two control points for generating a Bezier curve which is the spiral arm's curve

- a_4 and a_6 specify the angular distances of the points specified by a_3 and a_5
- a_7 to a_{11} specify the locations of five remaining microphones on the spiral arm's curve

The geometry of the generated arrays is then evaluated for how much it satisfies the desired geometry given by the main loop. Referring to the design vector $\mathbf{X}$, the array's geometry is specified in two aspects; the distribution density of microphones as a function of the array's radial distance, and the relationship between the microphone's radial distance with the distance to the nearest neighbor microphone.

The first aspect is evaluated as follows: Let the radial distance of the array be divided equally into n_{bin} statistical bins (intervals), each bin centers at the radial distance r_b, the microphone density distribution specified by X_1 and X_2 will determine the expected number of microphones in each bin. If N_{r_b} is the expected number of microphones in a bin centered at r_b and N'_{r_b} is the actual number of microphones in this bin of the generated array, the mismatch between the desired and actual number is $|N'_{r_b} - N_{r_b}|$.

The second aspect is evaluated for every microphone. Let the n^{th} microphone locate at the radial distance r_n measured from the array's center, the distance from this microphone to its nearest neighboring microphone specified by X_3 and X_4 is supposed to be d_{nn,r_n}. In the generated array, the distance from this microphone to its nearest neighbor is actually d'_{nn,r_n}. With this, the mismatch of the desired and the actual distance is $|d'_{nn,r_n} - d_{nn,r_n}|$.

The objective of the nested optimization loop is to minimize the summation of all aforementioned mismatches. The objective function for the nested optimization loop is defined as

$$J_{\text{nested}} = \frac{1}{n_{\text{bin}}} \sum_{b=1}^{n_{\text{bin}}} \frac{|N'_{r_b} - N_{r_b}|}{N_{r_b}} + \frac{1}{N} \sum_{n=1}^{N} \frac{|d'_{nn,r_n} - d_{nn,r_n}|}{d_{nn,r_n}}. \tag{21}$$

The summation in the first and second terms of Eq. (21) sums up the mismatches over all radial distance bins and microphones, respectively. The normalization in the summation normalizes the mismatch and allows both terms to be added. The division by n_{bin} and N ensure that the summation in both terms are having equal relative importance.

For the nested optimization loop, there is no known relationship between the design variables and the objective function. Moreover, multiple designs are desirable for a certain X to ensure the design flexibility. Due to these conditions, the *Differential Evolution* (DE) algorithm [19, 20] which is a variant of the Genetic Algorithm (GA) is implemented. The detailed explanation of the DE algorithm can be found in [5].

The structure of the optimization method is summed up in Table 1. This was implemented in a MATLAB program. Then optimization runs were executed.

4 OPTIMIZATION RESULTS

Figure 5 shows the scatter plots of $\overline{MLW}$ and $\overline{MSL_{\text{W}}}$ of all arrays evaluated in the optimization. The markers of the arrays generated by the initial and optimal design vectors ($\mathbf{X}$) are highlighted in red and blue, respectively. A marker showing the performance of the Underbrink array [21] is also shown. It can be seen that the performances of the arrays generated by the initial and

Table 1: Summary of the implemented optimization method

	Main optimization loop	Nested optimization loop
Design vector	**X** containing four design variables describing the array's geometric features	**a** containing eleven design variables used for defining microphone locations on a spiral arm in a multi-arm spiral array
Objective function	Equation (20) minimizing the MLW and weighted MSL	Equation (21) minimizing the mismatches between the array's actual and desired geometric features
Optimization algorithm	HJ/GPS	DE

optimal **X** are separated. A clear reduction of $\overline{MLW}$ can be seen. Almost all arrays generated by the optimal **X** have somewhat lower $\overline{MLW}$ and $\overline{MSL_W}$ than the Underbrink array[1].

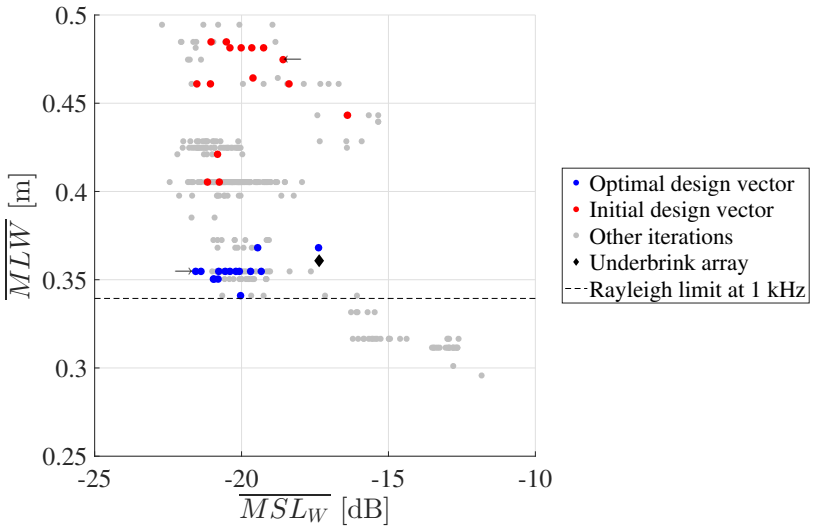

Figure 5: $\overline{MLW}$ and $\overline{MSL_W}$ of all array configurations considered in the optimization including the benchmarking Underbrink array, the arrows show the selected initial and optimal arrays

A candidate array is selected from the initial and optimal set of array designs for further investigations. These arrays are pointed by the arrows in Fig. 5. Let them be called the *initial* and *optimal* arrays. The Underbrink, initial, and the optimal arrays are shown in Fig. 6.

The unweighted MSL and MLW of the selected arrays at different beamforming frequencies when a point white noise source is simulated at 1.5 m away from the array are shown in Fig. 7. It can be seen that the MSL shows an increasing trend with the beamforming frequency while the MLW reduces with the beamforming frequency. At most beamforming frequencies, the MSL of the optimized array is somewhat lower than the Underbrink array. The low MSL

[1]Some averaged weighted MSLs ($\overline{MSL_W}$) are lower than -17.6 dB due to the weights applied.

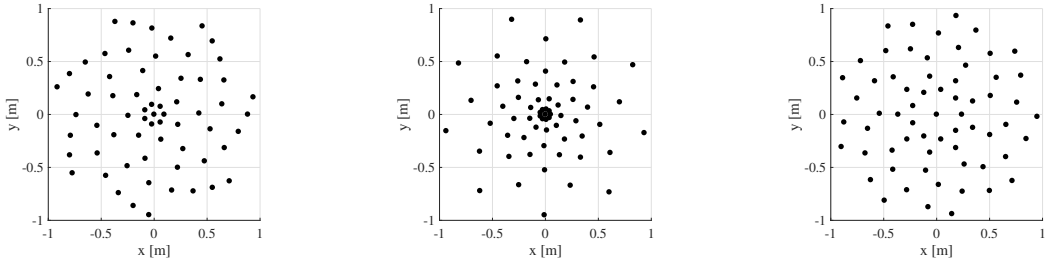

(a) Underbrink array (b) Initial array (c) Optimized array

Figure 6: Microphone arrays considered

values at the low beamforming frequencies result from the fact that the MLW is large at those frequencies, so most of the side lobes are not yet captured in the beamforming region.

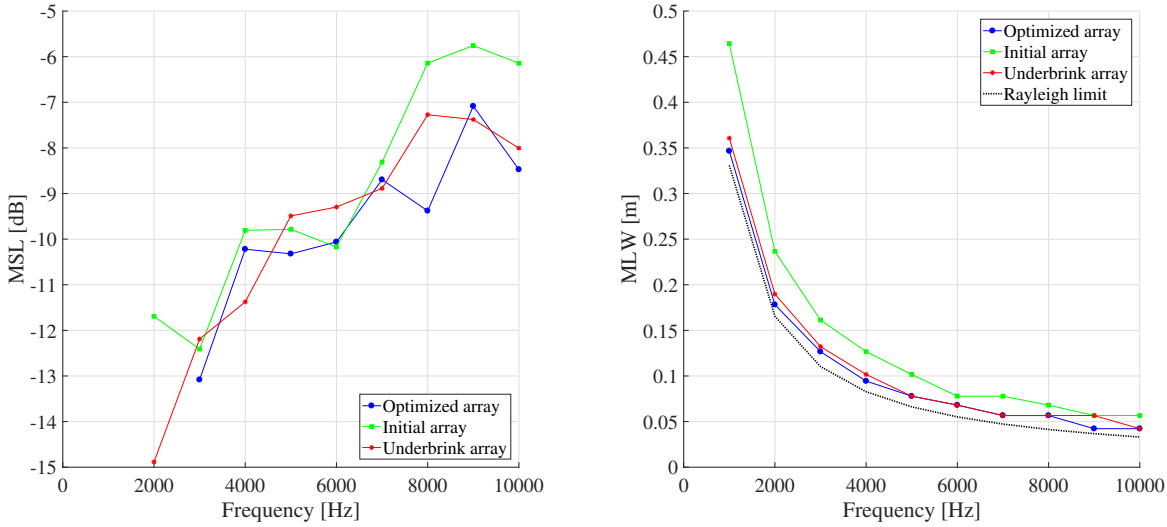

(a) MSL (b) MLW

Figure 7: MSL and MLW of the optimized array obtained from simulations compared with those from the initial and the Underbrink arrays

Interestingly, the MSL of the optimized array is higher than the Underbrink array at the beamforming frequency of 4 kHz. The source maps produced by beamforming of a single white noise source using the three arrays in Fig. 6 are shown in Fig. 8. It can be seen that, although the MSL of the optimized array is higher than the Underbrink array, the side lobes of the optimized array appear far away from the main lobe. The side lobe levels up to 0.5 m around the main lobe of the optimized array at 4 kHz are lower than -15 dB. These are the results of applying side lobe weighing. It is also notable that the MLW of the optimized array is comparable to the Underbrink array and lower than the initial array.

From this point on, only the optimized array is compared with the Underbrink array. The

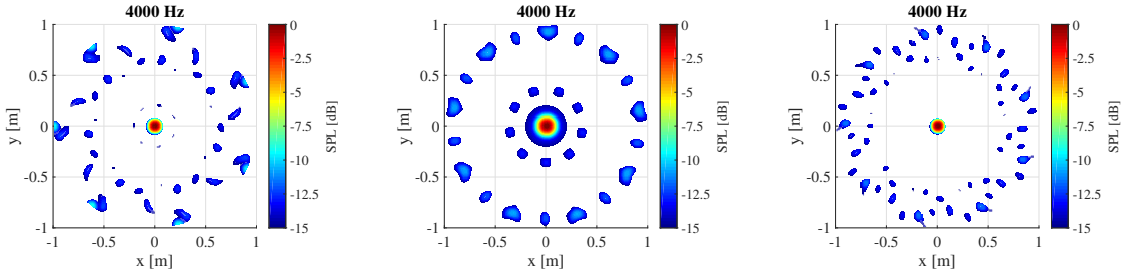

(a) Underbrink array (b) Initial array (c) Optimized array

Figure 8: Source maps from beamforming simulation of a single source at 4 kHz

ability of the optimized array to aid the HR CLEAN-SC algorithm in resolving two closely-spaced sources is investigated. Two incoherent point white noise sources are simulated with 10 cm separation at 1.5 m away from the array. With this setting, the Rayleigh limit in Eq. (16) suggests that the sources should be resolvable above the beamforming frequency of 3.3 kHz.

The resolvability of two closely spaced sound sources as a function of beamforming frequency can be anticipated by investigating a plot of the resolved SPL of the sources compared with the *exact* SPLs as done in [8]. At frequencies lower than the Rayleigh limit, the CLEAN-SC algorithm tends to overestimate the SPL of one source, and underestimate that of the other source with a wrong localization for both sources. Above the Rayleigh limit, the source localization and the their resolved SPLs converge to the correct values. The HR CLEAN-SC algorithm usually resolves two sound sources as one source with a slightly higher SPL up to a certain beamforming frequency, but below the frequency associated with the Rayleigh limit. After that point, the localization and SPL estimation of both sources get closer to the exact values. The frequency range from that certain frequency up to the Rayleigh limit is the improvement caused by the HR CLEAN-SC algorithm. Therefore, the lower the frequency where the resolved SPLs converge to the exact values, the larger the improvement is.

Plots showing the resolved SPLs of two closely spaced sources using the CLEAN-SC and HR CLEAN-SC algorithms with a constant $\mu = 0.25$ are shown in Fig. 9. The results from the Underbrink array and the optimized array are shown separately. The resolved values are compared with the exact values obtained by beamforming each source individually using the CLEAN-SC algorithm.

From both plots, it can be seen that the CLEAN-SC algorithm can resolve the sources only above the Rayleigh limit. The HR CLEAN-SC algorithm resolves the sources from a frequency slightly higher than 2000 Hz for the Underbrink array and slightly lower than 2000 Hz for the optimized array. Therefore, there is a slight improvement caused by the optimized array.

As explained earlier, the source marker constraint (μ) in the HR CLEAN-SC algorithm can be adjusted to improve the resolution. However, this needs to be done carefully to prevent the source marker from staying on the side lobes. It is observed from Fig. 9 that the source resolvability is critical at low frequencies. Fortunately, it is also observed that the MSL values are low at low frequencies as shown in Fig. 7(a). We can make use of this fact by adapting μ with beamforming frequency. It is assumed that the MSL is -17.5 dB at 100 Hz and increases linearly to -5 dB at 10000 Hz. With this assumption, the adaptive μ ($\mu(f)$) can be calculated for each frequency as

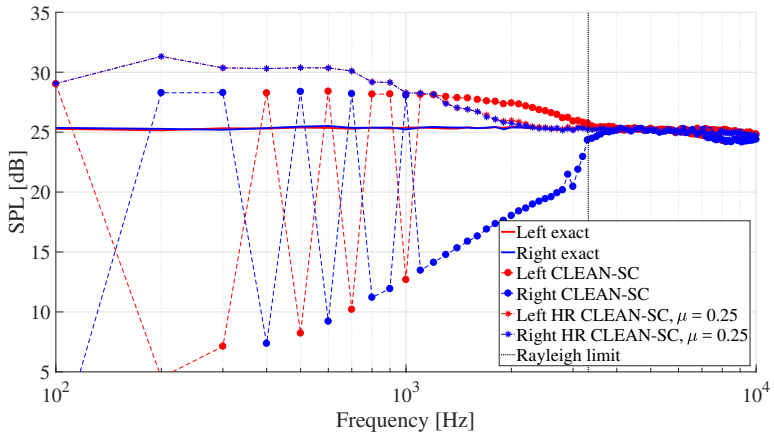

(a) Underbrink array

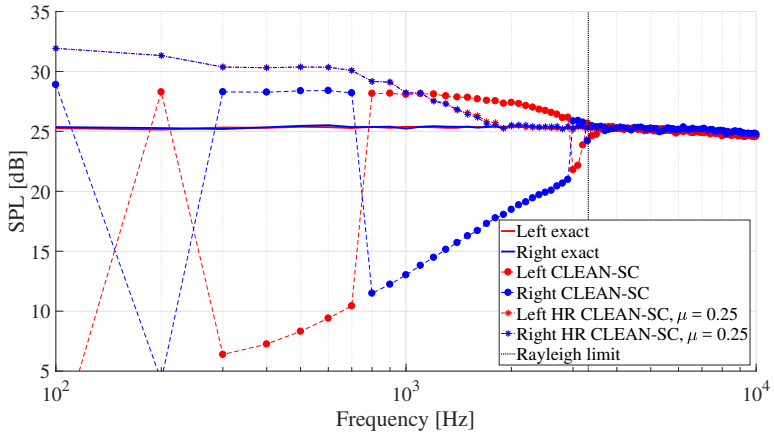

(b) Optimized array

Figure 9: Resolved SPL of two closely-spaced sound sources versus beamforming frequency, obtained from CLEAN-SC and HR CLEAN-SC beamforming simulations, compared with the exact SPL values

$$\mu(f) = 10^{MSL(f)/10}. \tag{22}$$

The curve of μ versus frequency is shown in Fig. 10. This is applied to the the same simulated data as in Fig. 9. The results are shown in Fig. 11. It can be seen that for HR CLEAN-SC, the resolved SPLs converge to a value close to the exact value at a lower frequency than the HR CLEAN-SC beamforming with a constant μ. Again, for the optimized array, this frequency is slightly lower than for the Underbrink array. Thus, the adaptive μ and an array with low MSL can help widen the frequency range where the beamforming resolution is improved by the HR CLEAN-SC algorithm.

Finally, the source maps produced by conventional beamforming, CLEAN-SC, HR CLEAN-SC with $\mu = 0.25$, and HR CLEAN-SC with adaptive μ, using the Underbrink and the optimized arrays at 1 kHz are shown in Fig. 12. The intersections of the dashed lines show the exact

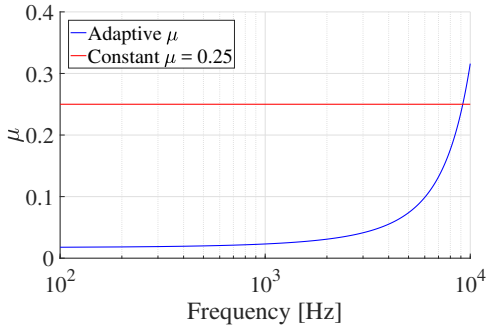

Figure 10: Values of adaptive μ used versus beamforming frequency

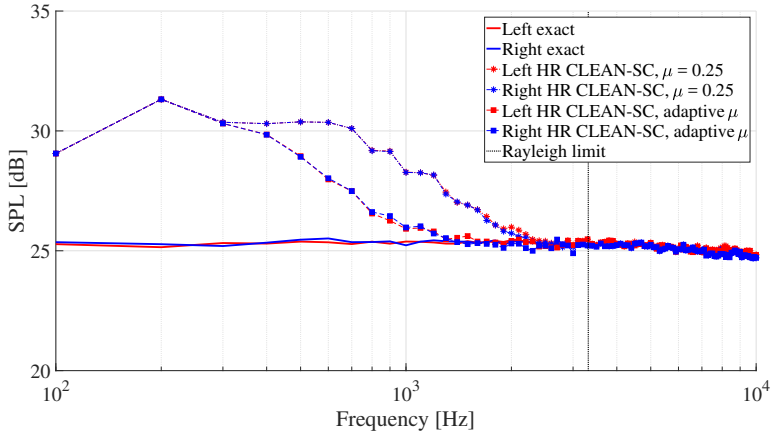

(a) Underbrink array

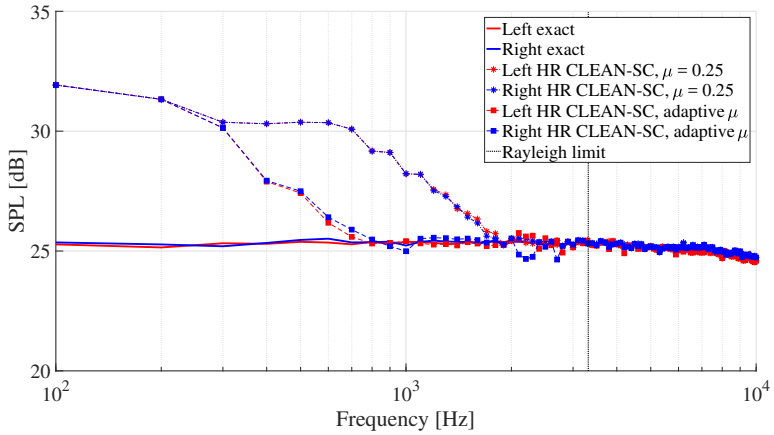

(b) Optimized array

Figure 11: Resolved SPL of two closely-spaced sound sources versus beamforming frequency, obtained from HR CLEAN-SC beamforming simulations with a constant and adaptive μ, compared with the exact SPL values

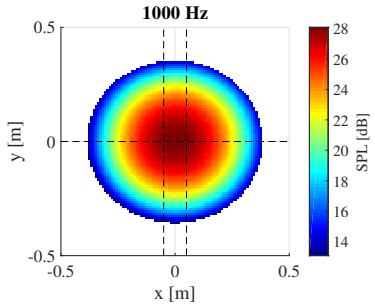

(a) Underbrink array, conventional beamforming

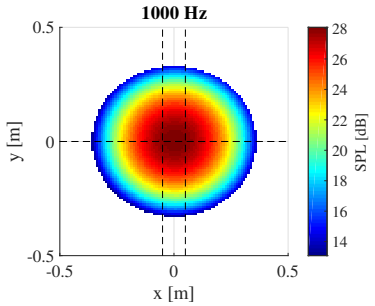

(b) Optimized array, conventional beamforming

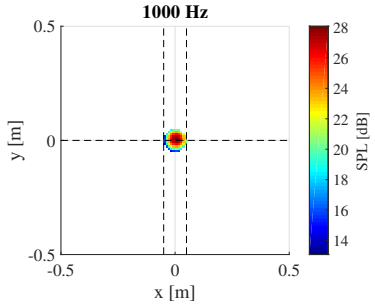

(c) Underbrink array, CLEAN-SC

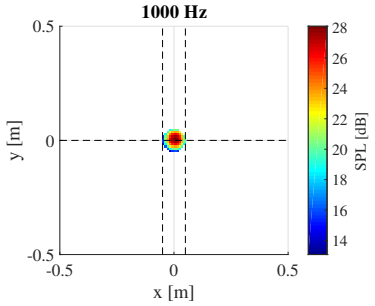

(d) Optimized array, CLEAN-SC

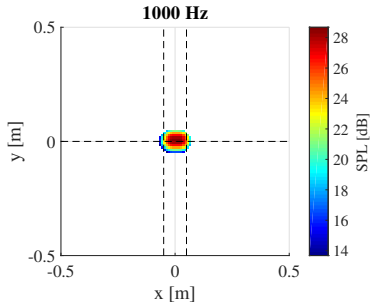

(e) Underbrink array, HR CLEAN-SC, $\mu = 0.25$

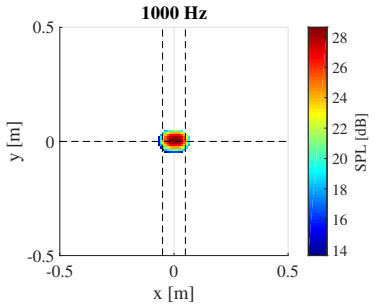

(f) Optimized array, HR CLEAN-SC, $\mu = 0.25$

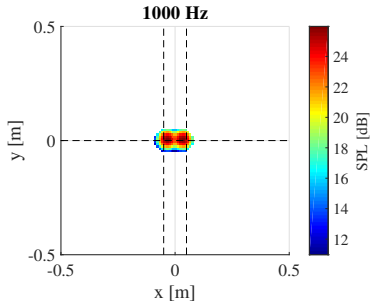

(g) Underbrink array, HR CLEAN-SC, adaptive μ

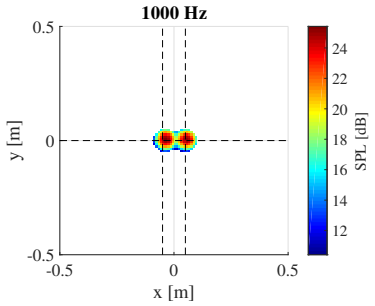

(h) Optimized array, HR CLEAN-SC, adaptive μ

Figure 12: Source maps of two closely-spaced sources for various beamforming algorithms at 1 kHz, using synthetic data

locations of the simulated sources. It can be seen that for conventional beamforming, CLEAN-SC, and HR CLEAN-SC with constant μ, the results from both arrays are similar, i.e. the sources are not resolved. On the other hand, two sources can most clearly be distinguished when the HR CLEAN-SC with adaptive μ is used with the optimized array.

5 EXPERIMENTAL VALIDATION

5.1 Experimental Set-up

Figure 13 shows the experimental set-up in the V-tunnel. The Underbrink and the optimized array were installed on a 2×2 m grid in the V-tunnel. Both arrays contain 64 G.R.A.S. 40PH Free-Field microphones. Since the actual grid contains a finite number of small microphone housing holes arranged in a square-lattice manner, the microphone configurations to be tested were adjusted to the closest housing holes.

Up to five Visaton K50 SQ speakers were used in the experiment. Each speaker emitted 30-second long white noise signals generated by MATLAB. The speakers were independently controlled. The signals played by each speaker were incoherent. To ensure the comparability of the results, the same speaker always played exactly the same signal file. The speakers were placed on a plane at 1.9 m away from the array in two arrangements as shown in Fig. 14. The following arrangements were considered:

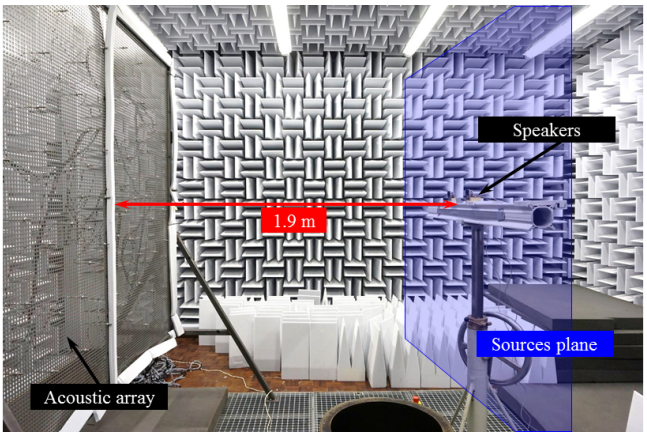

Figure 13: Experimental set-up in TU Delft V-tunnel

- Five-speaker arrangement: The speakers were placed adjacent to each other. The distance between the center of the speakers was 6.5 cm. By independently controlling the speakers, different source arrangements can be replicated. In this paper, the two following schemes are presented:
  - Single-source scheme: This was done by playing the signal using only the middle speaker.
  - Line source scheme: This was done by playing the signals using all the speakers. This scheme can replicate the line source, which is the frequently-encountered source configuration in aeroacoustics research, i.e. trailing-edge noise.

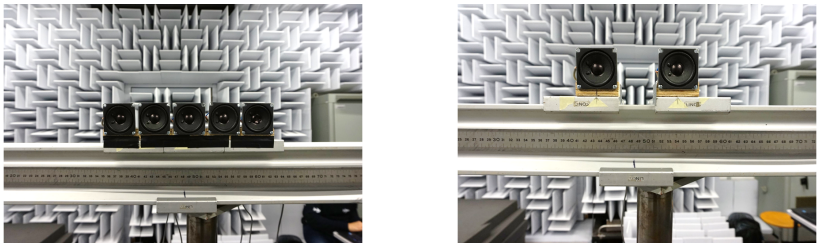

(a) Five-speaker arrangement (b) Two-speaker arrangement

Figure 14: Speaker arrangements used in the experiment

- Two-speaker arrangement: Two speakers were placed with varying separation from each other. The separation was varied from 6.5 cm (the minimum separation), to 10 cm, 20 cm, 30 cm, and 50 cm. With this, the ability of the array in separating two closely-spaced sources can be investigated. Additional recordings, where each speaker played the signal individually, were carried out to determine the exact SPL emitted by each speaker. To keep this section concise, only the results with 10 cm separation are shown.

The sampling frequency of the array's data acquisition system was 50 kHz. The length of the recorded signal per session is 30 seconds. The signal was then divided into 0.01 second chunks with a 50 % overlap. Then the Fourier transform was applied and the CSMs were constructed and averaged from all signal chunks. With this, the frequency resolution is 100 Hz.

5.2 Experimental Results

Five-speaker arrangement

The source maps obtained from the single-source scheme at 4 kHz using the Underbrink array and the optimized array are shown in Fig. 15. The corresponding source maps obtained from simulated data are also shown. The noise source and the microphone locations are simulated at exactly the same locations as in the experiment. By comparing the source maps from the experiment and the simulation, it can be seen that the MLW and the side lobe locations are well predicted by the simulation. However, the side lobe levels from the experiment appear to be slightly higher than those in the simulation. This could be due to the speaker's characteristics, i.e. not fully omnidirectional, and the fact that there is an offset between the anechoic chamber's ability to replicate the free-field condition and the ideal free-field condition.

The same finding is also reflected in Fig. 16 where the MSL and MLW from these source maps for frequencies ranging from 1 to 10 kHz are shown. Although the MSL of the optimized array is predicted to be lower than the Underbrink array by the simulation, the MSL of both arrays are comparable for almost all frequencies in the measurements.

The line source scheme is obtained when all five speakers play the signals. Source maps obtained from beamforming at 4 kHz using the Underbrink and the optimized arrays are shown in Fig. 17. It can be seen that, as a result of weighing the side lobes, the optimized array can provide an area with lower side lobe levels around the line source compared to the Underbrink array. The size of the region representing the sound sources, equivalent to the MLW, of both arrays are comparable. From this observation, it can be deduced that the features of the source

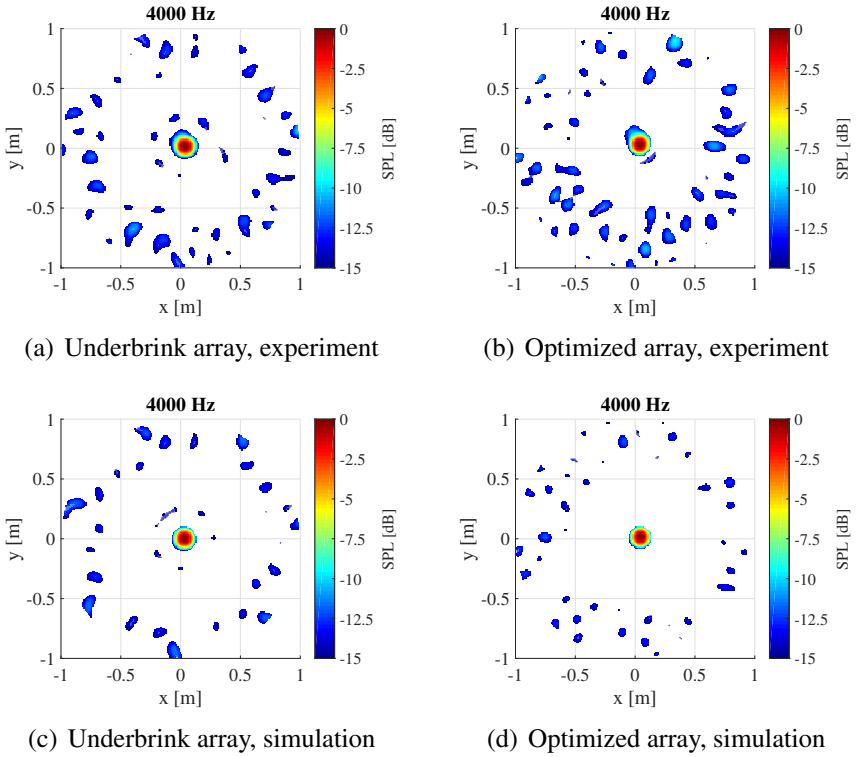

(a) Underbrink array, experiment

(b) Optimized array, experiment

(c) Underbrink array, simulation

(d) Optimized array, simulation

Figure 15: Source maps from beamforming of the five-speaker arrangement (single-source scheme) at 4 kHz compared with those from corresponding beamforming simulations

maps in the case of multiple sources produced by a certain array configuration will still follow the same trend as is observed in the single-source case of that particular array.

Two-speaker arrangement

Two speakers emitting incoherent white noise were placed with a separation of 10 cm at 1.9 m away from the optimized and the Underbrink array. With this setting, the Rayleigh limit in Eq. (16) suggests that the sources are resolvable at the frequencies above 4.2 kHz. The resolved sources' SPLs versus beamforming frequency using these two arrays and two beamforming algorithms (the CLEAN-SC and HR CLEAN-SC with $\mu = 0.25$) are shown in Fig. 18. The exact values are obtained from CLEAN-SC beamforming when only one source is playing the signal. The dashed line indicates the Rayleigh limit.

The behavior as observed in Fig. 9 can still be seen. Obviously, the CLEAN-SC algorithm can resolve both sources correctly at frequencies above the Rayleigh limit. However, the HR CLEAN-SC algorithm makes it possible for both sources to be resolved also at frequencies below the Rayleigh limit. The sources are resolved by both arrays from around 2000 Hz.

Further investigation is done by applying the adaptive μ (same as in Fig. 10) to this experimental data. The resolved source's SPLs by the HR CLEAN-SC algorithm with $\mu = 0.25$, adaptive μ, and the exact SPL values are shown in Fig. 19 for the Underbrink and the optimized

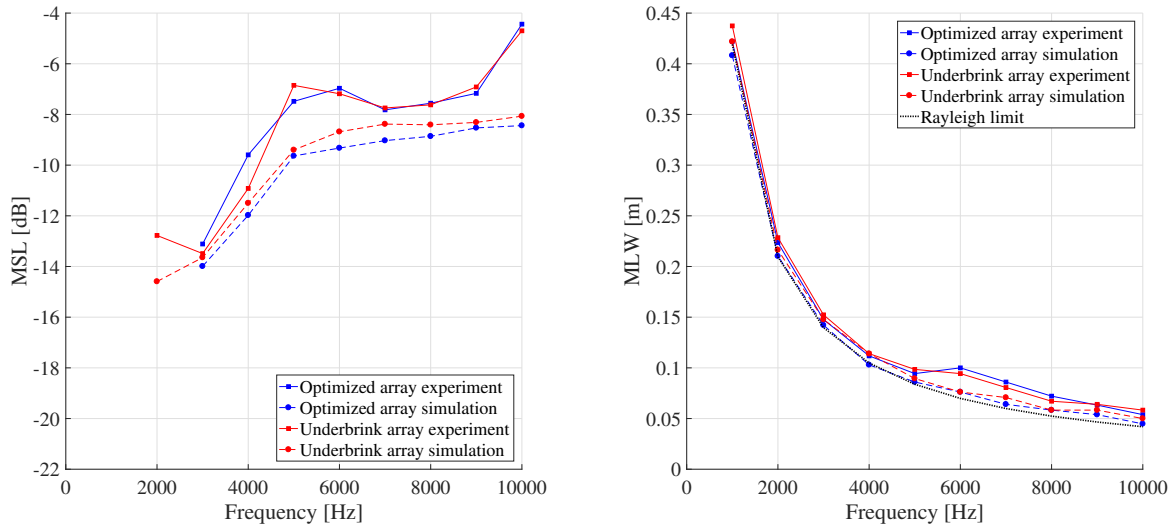

(a) MSL (b) MLW

Figure 16: MSL and MLW of the Underbrink and the optimized arrays from the experimental results compared with those obtained from simulations

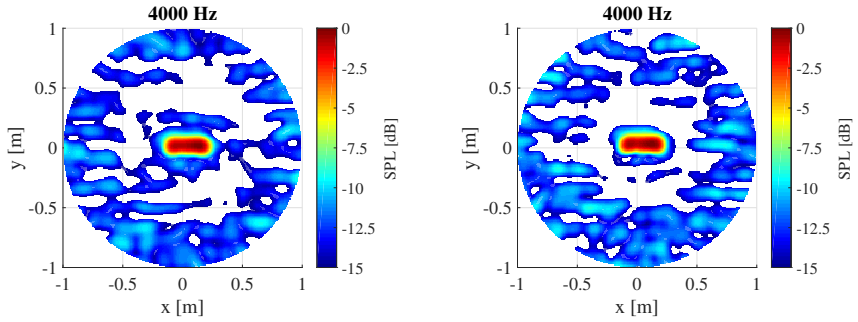

(a) Underbrink array (b) Optimized array

Figure 17: Source maps from beamforming of the five-speaker arrangement (line source scheme) at 4 kHz

array. Again, for both arrays, the adaptive μ makes the HR CLEAN-SC algorithm resolve the sources at a lower frequency than the constant μ case. The optimized array resolves the sources from around 600 Hz while the Underbrink array resolves the sources from around 1000 Hz.

Finally, the source maps produced by both arrays using the conventional beamforming, the CLEAN-SC algorithm, the HR CLEAN-SC algorithm with $\mu = 0.25$, and the HR CLEAN-SC algorithm with adaptive μ at 800 Hz are shown in Fig. 20. The intersections of the dashed lines indicate the centers of the speakers. As expected, this frequency is lower than the Rayleigh limit, the conventional beamforming fails to resolve the sources while the CLEAN-SC and HR CLEAN-SC algorithms resolve both sources with overestimated SPLs. Only the HR-CLEAN-

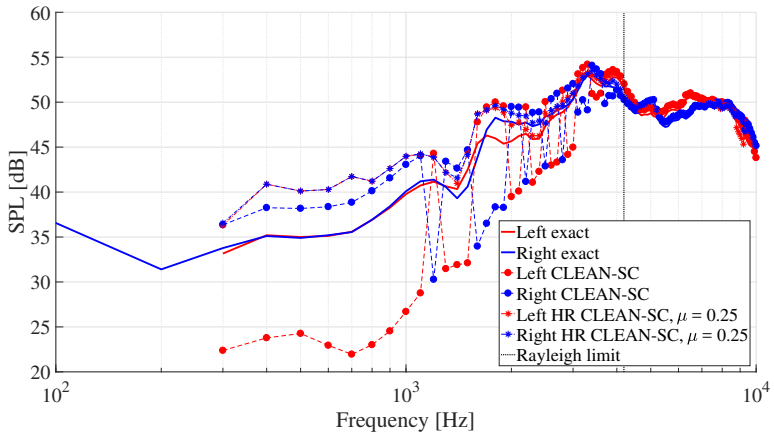

(a) Underbrink array

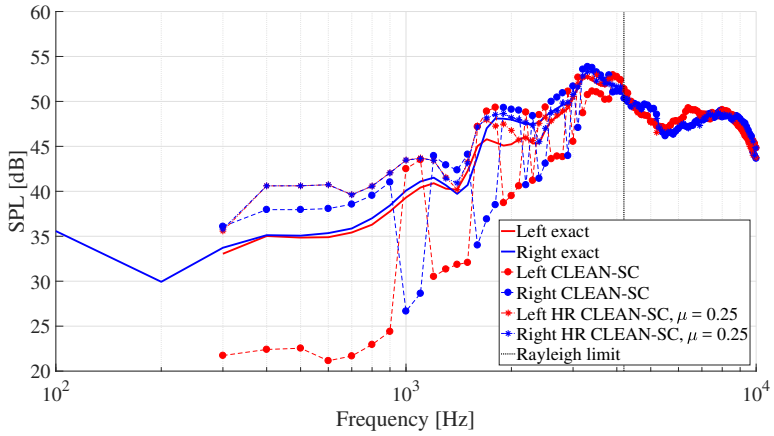

(b) Optimized array

Figure 18: Resolved SPLs of two sound sources with 10 cm separation versus beamforming frequencies, obtained from CLEAN-SC and HR CLEAN-SC beamforming of experimental data, compared with the exact SPL values

SC algorithm using the optimized array with adaptive μ can clearly resolve two sound sources. Source localization offsets can be seen. This could be due to the fact that the source is not a perfect point source and the maximum SPL at 800 Hz might be dominantly emitted by a certain part of the speakers.

6 CONCLUSIONS AND RECOMMENDATIONS

In this paper, the microphone configuration has been optimized for an acoustic array in an open-jet anechoic wind tunnel. The effects of the optimized design on the performance of the High-Resolution (HR) CLEAN-SC beamforming algorithm have been investigated.

The proposed optimization method focuses on using a minimal number of design variables. The optimization aims to reduce both the Main Lobe Width (MLW) and Maximum Side lobe

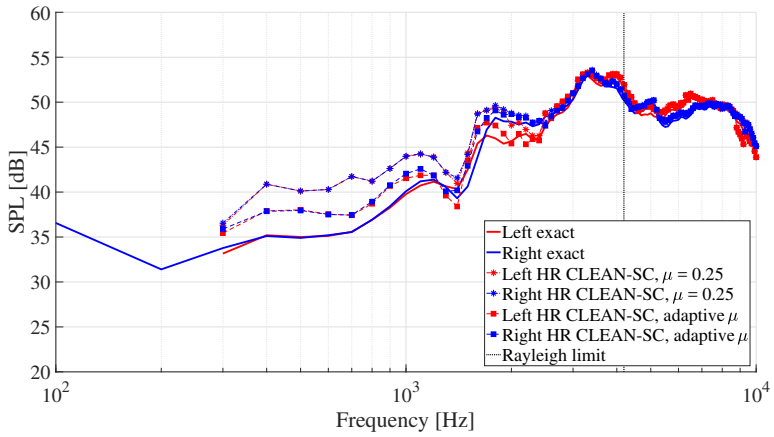

(a) Underbrink array

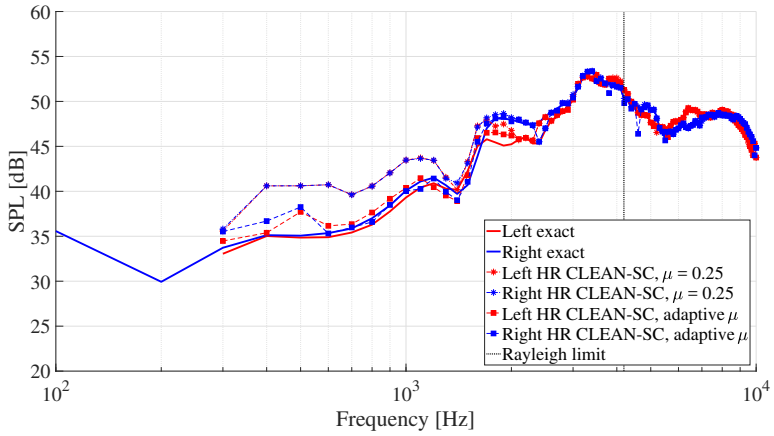

(b) Optimized array

Figure 19: Resolved SPL of two sound sources with 10 cm separation versus beamforming frequency, obtained from HR CLEAN-SC beamforming of experimental data with a constant and adaptive μ, compared with the exact SPL values

Level (MSL). The weights are applied to the side lobes according to their distances from the main lobe. This resulted in a region with side lobe levels lower than -15 dB around the main lobe. Low MLW has also been maintained.

The fact that the array design gives low side lobe levels can be further exploited by the HR CLEAN-SC algorithm. It was found that, when the optimized array is used to resolve two closely-spaced sound sources using the HR CLEAN-SC algorithm with an adaptive source marker constraint (μ), the two sources can be resolved in the broadest range of frequency below the Rayleigh limit.

Two recommendations can be given based this study. First, only attempting to minimize the MSL may not be sufficient for designing an acoustic array since the location of the side lobes also matters. In this study, the side lobes are associated with their distances from the main lobe through weighing. The produced source maps both from conventional beamforming and the

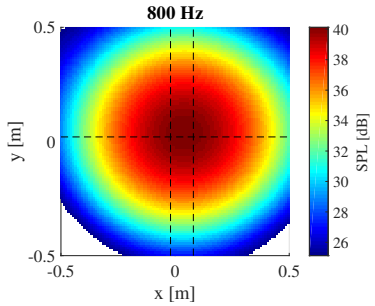

(a) Underbrink array, conventional beamforming

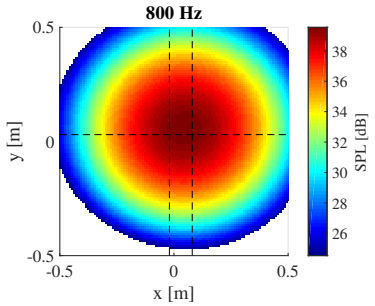

(b) Optimized array, conventional beamforming

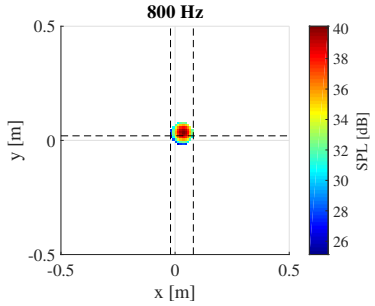

(c) Underbrink array, CLEAN-SC

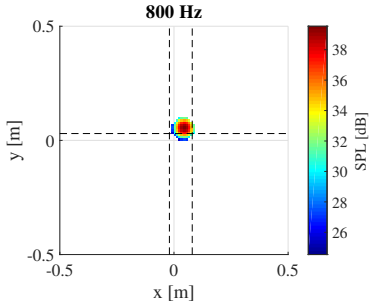

(d) Optimized array, CLEAN-SC

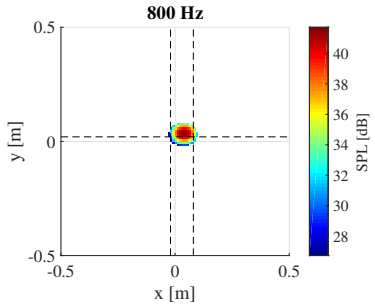

(e) Underbrink array, HR CLEAN-SC, $\mu = 0.25$

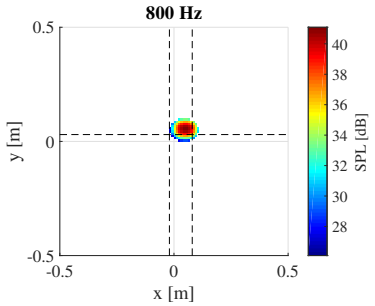

(f) Optimized array, HR CLEAN-SC, $\mu = 0.25$

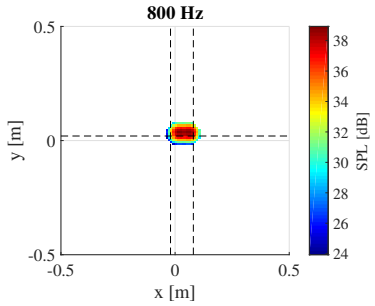

(g) Underbrink array, HR CLEAN-SC, adaptive μ

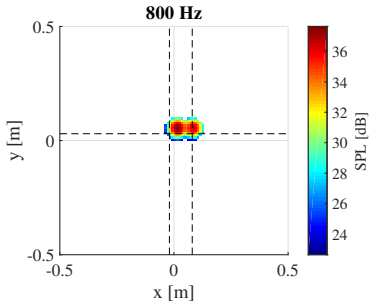

(h) Optimized array, HR CLEAN-SC, adaptive μ

Figure 20: Source maps of two closely-spaced sources for various beamforming algorithms at 800 Hz, using experimental data

advanced beamforming algorithms show satisfactory results. Second, to best exploit the ability of the HR CLEAN-SC algorithm, the source marker constraint (μ) should be adjusted according to the MSL at the frequency of interest. This should be done especially at the frequencies below the Rayleigh limit where the source resolvability is low, but the side lobe levels are generally low as well.

REFERENCES

[1] D. G. Simons, M. Snellen, B. van Midden, M. Arntzen, and D. Bergmans, "Assessment of noise level variations of aircraft flyovers using acoustic arrays," *Journal of Aircraft*, 2015.

[2] S. Oerlemans, L. Broersma, and P. Sijtsma, "Quantification of Airframe Noise Using Microphone Arrays in Open and Closed Wind Tunnels," *Int. J. Aeroacoustics*, vol. 6, no. 4, pp. 309–333, 2007.

[3] T. Geyer, E. Sarradj, J. Giesler, and M. Hobracht, "Experimental assessment of the noise generated at the leading edge of porous airfoils using microphone array techniques," in *17th AIAA/CEAS Aeroacoustics Conference (32nd AIAA Aeroacoustics Conference)*, June 2011.

[4] E. Sarradj, "A generic approach to synthesize optimal array microphone arrangements," in *Proceedings of the 6th Berlin Beamforming Conference*, 2016.

[5] A. Malgoezar, M. Snellen, P. Sijtsma, and D. Simons, "Improving beamforming by optimization of acoustic array microphone positions," in *Proceedings of the 6th Berlin Beamforming Conference*, pp. 1–24, 2016.

[6] F. Le Courtois, J.-H. Thomas, F. Poisson, and J.-C. Pascal, "Genetic optimisation of a plane array geometry for beamforming. application to source localisation in a high speed train," *Journal of Sound and Vibration*, vol. 371, pp. 78–93, 2016.

[7] Z. Prime, C. Doolan, and B. Zajamsek, "Beamforming array optimisation and phase averaged sound source mapping on a model wind turbine," in *Inter-Noise and Noise-Con Congress and Conference Proceedings*, vol. 249, pp. 1078–1086, Institute of Noise Control Engineering, 2014.

[8] P. Sijtsma, R. Merino-Martinez, A. Malgoezar, and M. Snellen, "High-resolution clean-sc: theory and experimental validation," in *23rd AIAA/CEAS Aeroacoustics Conference*, p. 3841, 2017.

[9] P. Sijtsma, "CLEAN based on spatial source coherence," *International Journal of Aeroacoustics*, vol. 6, pp. 357–374, 2007.

[10] Z. Prime and C. Doolan, "A comparison of popular beamforming arrays," *Australian Acoustical Society AAS2013 Victor Harbor*, vol. 1, p. 5, 2013.

[11] N. Jin and Y. Rahmat-Samii, "Advances in particle swarm optimization for antenna designs: Real-number, binary, single-objective and multiobjective implementations," *IEEE Transactions on Antennas and Propagation*, vol. 55, no. 3, pp. 556–567, 2007.

[12] R. L. Haupt, "Thinned arrays using genetic algorithms," *IEEE Transactions on Antennas and Propagation*, vol. 42, no. 7, pp. 993–999, 1994.

[13] J. Yu and K. D. Donohue, "Geometry descriptors of irregular microphone arrays related to beamforming performance," *EURASIP Journal on Advances in Signal Processing*, vol. 2012, no. 1, p. 249, 2012.

[14] E. Sarradj, "Three-dimensional acoustic source mapping with different beamforming steering vector formulations," *Advances in Acoustics and Vibration*, vol. 2012, no. 292695, pp. 1–12, 2012.

[15] R. P. Dougherty, "Beamforming in Acoustic Testing," in *Aeroacoustic Measurements* (T. J. Mueller, ed.), ch. 2, pp. 62–97, Springer-Verlag Berln Heidelberg New York, 2002.

[16] V. Torczon, "On the convergence of pattern search algorithms," *SIAM Journal on optimization*, vol. 7, no. 1, pp. 1–25, 1997.

[17] R. Hooke and T. A. Jeeves, ""direct search"solution of numerical and statistical problems," *Journal of the ACM (JACM)*, vol. 8, no. 2, pp. 212–229, 1961.

[18] R. M. Lewis and V. Torczon, "Pattern search algorithms for bound constrained minimization," *SIAM Journal on Optimization*, vol. 9, no. 4, pp. 1082–1099, 1999.

[19] R. Storn and K. Price, "Differential evolution–a simple and efficient heuristic for global optimization over continuous spaces," *Journal of global optimization*, vol. 11, no. 4, pp. 341–359, 1997.

[20] M. Snellen and D. G. Simons, "An assessment of the performance of global optimization methods for geo-acoustic inversion," *Journal of Computational Acoustics*, vol. 16, no. 02, pp. 199–223, 2008.

[21] J. R. Underbrink, "Circularly symmetric, zero redundancy, planar array having broad frequency range applications," Mar. 20 2001. US Patent 6,205,224.